Tunable oscillations in the Purkinje neuron

Ze'ev R. Abrams,[1,2] Ajithkumar Warrier,[1] Yuan Wang,[1] Dirk Trauner,[3] and Xiang Zhang[1,2,4,*]

[1]*NSF Nanoscale Science and Engineering Center, 3112 Etcheverry Hall, University of California, Berkeley, California 94720, USA*

[2]*Applied Science & Technology, University of California, Berkeley, California 94720, USA*

[3]*Department of Chemistry and Biochemistry, Ludwig-Maximilians-Universität München (LMU),*
Butenandtstrasse 5–13, 81377 Munich, Germany

[4]*Material Sciences Division, Lawrence Berkeley National Laboratory, Berkeley, California 94720, USA*

In this paper, we experimentally study the dynamics of slow oscillations in Purkinje neurons *in vitro*, and derive a strong association with a forced parametric oscillator model. We observed the precise rhythmicity of these oscillations in Purkinje neurons, as well as a dynamic tunability of this oscillation using a photoswitchable compound. We found that this slow oscillation can be induced in every Purkinje neuron measured, having periods ranging between 10 and 25 s. Starting from a Hodgkin-Huxley model, we demonstrate that this oscillation can be externally modulated, and that the neurons will return to their intrinsic firing frequency after the forced oscillation is concluded. These findings signify an additional timing functional role of tunable oscillations within the cerebellum, as well as a dynamic control of a time scale in the brain in the range of seconds.

I. INTRODUCTION

The Purkinje neuron (PN) is the largest neuron in the cerebellum, with over 100,000 inputs and a single output axon [1,2]. Due to its geometry and orientation in the cerebellum, it has been cited as a possible integrator for the motor control system of the brain [2], with many basic neuroscience and artificial intelligence theories based on its complex neuronal network [3,4]. While most studies of the PN focus on biological sources of memory (plasticity) [5,6], a number of studies also describe the functionality of the cerebellum in terms of independent oscillators [6–8].

We have previously reinforced this set of theories with an experimental study demonstrating the intrinsic firing characteristics of the PN [9,10]. We identified three frequency bands inherent to the PN, which we denoted as the sodium (Na^+; >30 Hz), calcium (Ca^{2+}; 1–10 Hz), and switching bands (<1 Hz). This set of frequency bands is distinct from other regions of the brain [11–14], with the "switching" frequency described and measured for the first time [9]. This switching frequency operates at lower frequencies than those typically associated with memory and other cerebellar processes [14]; however, there have recently been parallel *in vivo* experiments that have demonstrated similar slow oscillations between 0.039 and 0.078 Hz [15]. We have used the terminology of digital circuits and nonlinear oscillators to describe the switching from rapid firing to quiescence as an *astable* mode, which oscillates between the "on" and "off" states in a rhythmic pattern, without maintaining any single state indefinitely ("astable") [10]. This is in contrast with the known *bistable* mode in the PN [16–18], where the firing rate can be toggled between firing and quiescence and maintains that state indefinitely; or a *monostable* mode where the PN has been shown to fire rapidly *in vivo* with only brief pauses [19]. These three modalities are intrinsically linked, and we have postulated that a system exhibiting one of these modes will likely display the other modes under certain conditions [10].

This paper attempts to validate this claim by focusing entirely on the astable mode of firing.

In this paper, we first show that every PN measured here *in vitro* can exhibit this slow form of astable oscillation when activated using pharmacological compounds. These slow oscillations are shown to be precise, maintaining the same rhythmic oscillation frequency over time with high quality factors of resonance. While we had previously described some cells displaying this oscillatory switching when measured *in vitro*, we show that this mode can be activated in every cell measured, thereby indicating an inherent functional role. Next, we modulate the frequency of these neurons using a unique form of highly specific, photoswitchable compound [20]. By doing this, we show that this frequency pattern acts as a forced oscillator when externally driven, and that the oscillations revert back to their initial frequency once the driving force is stopped. Using the Hodgkin-Huxley neuron model [21], we derive a form of parametric oscillator that describes the slow oscillations observed, as well as their ability to be externally tuned. Finally, we analyze the parameters of oscillation, and compare them with the existing literature to further understand the gating mechanism controlling this oscillation behavior of Purkinje neuron cells. The results are summarized in terms of neuronal oscillation models and cerebellar timing functions.

II. METHODS

Animal handling and care was done according to guidelines set by the Office of Laboratory Animal Care (OLAC) at UC Berkeley. Sprague-Dawley rats (aged 21 to 30 days) were initially euthanized using isoflurane and then decapitated. Their cerebella were isolated and 250-μm-thick parasagittal slices were obtained using a vibratome (Leica VT1000s) while submerged in a sucrose-based slicing media. Brain slices were transferred to an incubation chamber containing artificial cerebrospinal fluid (ACSF) bubbled with carboxygen (95% O_2/5% CO_2) held at 37 °C for 1–4 h prior to experiment. For a complete description of sample preparation, solutions used, and the optical patch-clamp setup, please refer to [9], which matched the experimental conditions here exactly.

*Xiang@berkeley.edu

The stimulation of PNs was done by activating kainate receptors using a variety of highly selective molecular kainate receptor agonists (KRAs). These molecules act only upon kainate receptors without activating any of the other glutamatergic receptors on the cell, particularly AMPA (α-amino-3-hydroxyl-5-methyl-4-isoxazole-propionate) receptors, which are the majority of ionotropic glutamatergic receptors on PNs. Additional pharmacological blockers were used to isolate the kainate response in the PN. The photoswitchable kainate receptor agonist (PSKRA) [20] was used as a traditional KRA when in the dark. The photoresponse is described in Ref. [20], as well as in the text.

All drugs except the PSKRA were purchased via Sigma-Aldrich or Tocris Bioscience. Drugs were applied to the ACSF reservoir and allowed to perfuse onto the slice using a closed-loop system. Kainate activation of the PNs was achieved using either highly specific KRAs, or monosodium glutamate (MSG, 100 μM) in conjunction with an AMPA receptor blocker GYKI-52466 (10–20 μM). The KRAs used consisted of the commercially available (2S,4R)-4-methylglutamic acid (SYM-2081, 10–50 μM), a nonselective GluK1/GluK2 agonist (nonselective for GluR5/6, selective over AMPA receptors), as well as the PSKRA. The PSKRA was based upon a variant of the commercially available SYM-2081, called LY339434 [22], which was designed specifically to be selective towards GluK1 (GluR5) over both GluK2 (GluR6) and AMPA receptors, and was used at 50–100 μM, the ideal concentration as described in Ref. [20].

Additional network activity upon the cell was removed via the application of tetrodotoxin (TTX, 1 μM), which blocks most synaptic activity by silencing Na^+ induced action potentials. Inhibitory synaptic transmission was blocked in some cells via the application of both ionotropic and metabotropic GABA blockers [$GABA_A$ was blocked with GABAzine (SR-95531), 10 μM, or picrotoxin, PTX, 100 μM, and $GABA_B$ with 5-bis(1,1-dimethylethyl)-4-hydroxy-a,a-dimethylbenzenepropanol (CGP, 20 μM)], as well as blocking glycine (strychnine, 1 μM). (RS)-a-methyl-4-carboxyphenylglycine (MCPG, 500 μM) was used to block mGluR1/2 metabotropic receptors. Despite the PN having no N-methyl-D-aspartic acid (NMDA) receptors, the possible presynaptic release of glutamate via NMDA receptors on the parallel fibers was preempted via the application of D-($-$)-2-amino-5-phosphonopentanoic acid (APV, 50 μM). Complete blocking of excitatory glutamatergic inputs to the cell was done by adding and 6,7-dinitroquinoxaline-2,3(1H,4H)-dione (DNQX, 10 μM), which blocks both AMPA and kainate receptors. For each of these network activity blocking experiments, at least $n = 2$ cells were measured with the compounds listed above.

Data analysis was done using a combination of PCLAMP (Molecular Devices, Inc.), Microsoft Excel, and MATLAB (Mathworks, Inc.) software. Patch-clamp sampling was done at 10 kHz, and then decimated to 1 kHz for data analysis. Period/duty-cycle (DC) tracking was implemented using a custom code. The periods/DCs were tracked over time by selecting overlapping windows in time (30–60 s each, different for each cell), and collecting the start and stop times for spike bursts. "Off" times were defined as any period longer than 2 s, and the DC was calculated as the "On" times divided by the

full period (measured as the time between Off cycles, or On cycles, within each window). Time-constant (τ) evaluation of the forced modulation via the PSKRA was done using the MATLAB Curve Fitting Toolbox. The fitting was done on a basic, time-shifted exponential decay function, of the form $x(t) = x_f - \Delta x / \exp[-(t - t_0)/\tau]$, with the parameters dependent upon the data.

Fast Fourier transforms (FFTs) were done using standard MATLAB functions. The confidence intervals on the spectrum were found by fitting a Gaussian function to the peak using the Curve Fitting Toolbox in MATLAB. This fitting provided the 95% confidence intervals of the fit, which were plotted in Fig. 2. The deviation of the oscillation frequency (in Fig. 2) can also be measured by the full width at half maximum (FWHM) as well as by fitting the Gaussian to obtain the standard deviation. For a Gaussian fitting of the peak, the standard deviation (SD) or σ is σ = FWHM/2.354. Broader peaks indicate higher fluctuations in the frequency. The quality factor Q of a resonator/oscillator is the ratio between the peak measured and the FWHM, which is an equivalent measure to its signal to noise ratio (SNR), or the reciprocal of the coefficient of variation.

III. RESULTS

A. Induction of astability

We first demonstrate that PN will change its firing pattern to that consisting of slow oscillations of Ca^{2+} spikes [23], nested within a slow switching envelope wave, when measured *in vitro* using a current-clamp setup. Figures 1(a) and 1(c) display the recordings of two cells transitioning to this mode after the application of KRAs in conjunction with tetrodotoxin (1 μM), which abolishes the Na^+ spikes, and accentuates the underlying Ca^{2+} spike pattern, as well as an AMPA receptor blocker (GYKI, 10 μM). The transition to a slow oscillation mode consisting of switching and calcium frequencies occurs after 0.5–2 min (green line in dotted box), after which a clear oscillation pattern is shown (gray line in dashed box). Once induced into this slow oscillation mode, the system retains its rhythmic astability, with cells oscillating between firing Ca^{2+} spikes and quiescence for up to 40 min in some cells. The oscillation frequency can be measured from the highest peak in the FFT of the recording, as shown in Figs. 1(b) and 1(d) below each recording. The sharp peaks in the FFT signify a clear oscillation frequency. The existence of some low-frequency peaks in the initial firing pattern in Fig. 1(d) reveal that this low frequency was inherent to the cells, even before induction into the astable mode via KRAs [9]. Results such as those displayed in Fig. 1 were obtained in $n > 50$ cells, with induction into the astable mode occurring in nearly all of the cells measured, signifying the reproducibility of these results. Induction of astability was possible using both the PSKRA in the dark ($n > 50$), as well as by using the commercially available compound SYM-2081 ($n = 8$) from which the PSKRA was derived, as well as using standard MSG in conjunction with blocking the AMPA receptors ($n = 3$ of 5 cells; this method was less preferable due to the initiation of a depolarization block at high doses of MSG, 100 μM). The SYM-2081 was used to verify that the result was reproducible to other methods of kainate
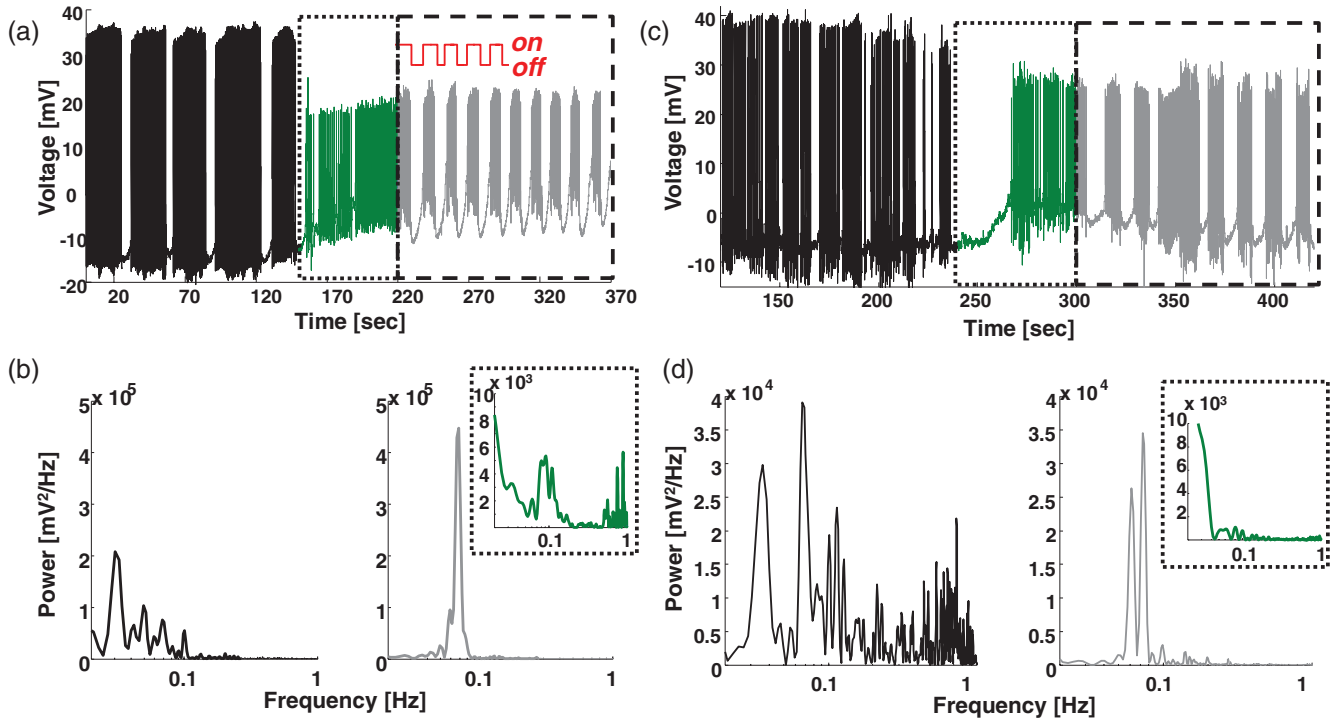
FIG. 1. (Color online) Astability induction in a Purkinje neuron. [(a), (c)] Signal output recordings of cells transitioning to an astable oscillatory mode after applying a kainate receptor agonist (PSKRA, 100 μM) in conjunction with an AMPA receptor blocker (GYKI, 10 μM) and Na^+ channel blocker (TTX, 1 μM). Clear oscillations are at the far right (gray line in dashed box), after a short transition period (green line in dotted box). Inset: analogy between the astable firing/quiescence pattern with a digital oscillator switching between two states [(b), (d)] Fourier transforms (power spectra) of the recordings before (black), during (green inset), and after (gray) the induction of oscillations (logarithmic x axis). A clear peak at 0.075 Hz can be seen in (b), whereas a split peak centered at 0.07 Hz is seen in (d), signifying a transition between two frequencies for this wave form. The transition period of the cell in (a) contained some low-frequency signatures, whereas the transition period in (c) contained nearly no low-frequency signature (other than zero-frequency noise).

activation, and not an artifact of the photoswitchable moiety of the PSKRA.

The frequency of the astable oscillations can be measured by tracking the on/off transitions in time using a windowing algorithm (see Methods), or directly by measuring the low-frequency peak in the Fourier transform. This is shown in Figs. 2(a) and 2(e) for two cells already induced into the astable mode using different pharmacological methods. In both recordings, a clear oscillation is seen for long periods of time (9 and 5.5 min, respectively). The oscillation is shown in Fig. 2(e) to consist of a sequence of Ca^{2+} spike bursts, occurring even when the Na^+ spikes are blocked with TTX. Tracking the slow oscillation cycles in the time domain [Figs. 2(b) and 2(f)] provide the average period (solid red line) and standard deviation (SD, dashed gray line) in a directly visible manner. In the frequency domain, the FFT provides all frequency information about the signal [Figs. 2(c) and 2(g)], including higher frequency Ca^{2+} and Na^+ spikes (if they are present). The low-frequency peak is best seen when no smoothing is added to the power spectrum, and the signal is zero padded for higher resolution. This allows a direct measure of the standard deviation (or FWHM) of the peaks in the bottom of Figs. 2(d) and 2(h), when fitted with single Gaussians. Drifts and shifts in the central frequency produce a broadening of the

peaks in the FFT, as well as the possibility of multiple peaks appearing in the spectrum [as in Fig. 2(d)].

B. Tunability via photoswitching

Until now we have shown only the natural astability frequencies measured in PNs after pharmacological induction; this induction of astability is comparable to the naturally occurring switching frequencies seen in control *in vitro* experiments [9]. Presently, we show that the PN can act as a *forced* oscillator, and thus extends the frequency range available for oscillations. This tunability can allow the PNs to produce a wider range of frequencies per cell, which can then be integrated together in other regions of the cerebellum [10], [24]. Using the PSKRA and the appropriate photoswitching wavelengths, shown in Fig. 3(a), we can gradually toggle the firing of Ca^{2+} spike bursts in a PN to a given oscillation period [Fig. 3(b)]. We observed that the firing pattern then matches the period of forced modulation. This was done at a wide range of periods (6–30 s) and duty cycles (DCs, 25%–75%).

The tunability of cells using the PSKRA was effective in all cells measured, with the slow oscillations following the forced photomodulation. Additionally, in a few of the cells that did not exhibit astability initially when in the presence of the
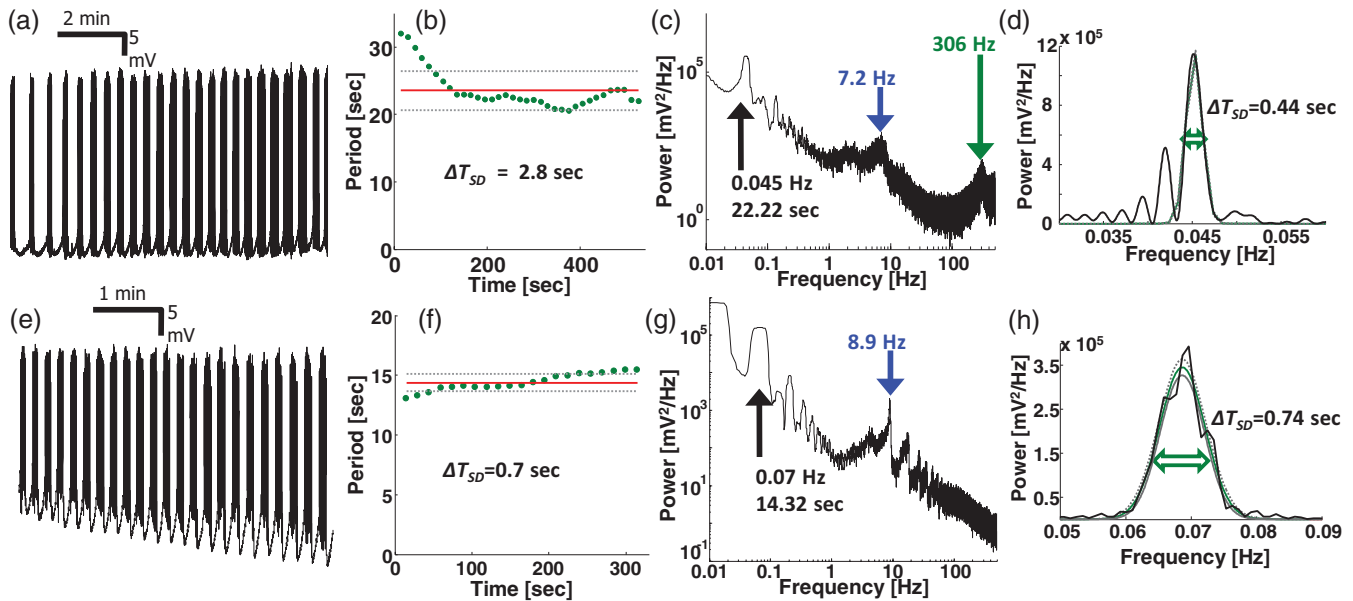
FIG. 2. (Color online) Measuring the induced oscillations. (a) 9 minute recordings of a cell induced to oscillate via application of glutamate (MSG, 100 μM) and an AMPA receptor blocker (GYKI, 10 μM). (b) The period of oscillation of bursts can be tracked over time to provide the average period (solid red line) and standard deviation (dashed gray line). (c) The smoothed power spectrum provides all frequency information of the recording, including calcium and sodium frequency modes [blue (dark gray) and green (light gray) arrows, respectively]. (d) Close-up of the low-frequency peak, with no smoothing to the spectrum, displaying multiple peaks, which account for the drift and shift in frequency. The central peak is fitted with a single Gaussian [green (light gray) line] with 95% confidence levels (dashed gray line), providing the standard deviation. (e) 5.5 minute recording after the application of PSKRA, GYKI, and TTX (100, 10, and 1 μM, respectively), which blocks the Na$^+$ spikes, as is seen in the lack of high-frequency activity in the power spectrum (g). The standard deviation in (h) matches that of (f) since the single Gaussian fit is more accurate for this signal.

PSKRA in the dark ($n = 5$), the photomodulation still resulted in forced oscillation, with the cells continuing to oscillate after the photoswitching was stopped, as demonstrated in Fig. 3(c).

We therefore differentiate between two effects described above: the *induction* of astability via the KRAs, which was possible using both the PSKRA and commercially available KRAs, and the *tunability* of the astability, which we show in Fig. 3 to be reliably effective using the PSKRA. The attachment of the PSKRA to the kainate receptors [25] (specifically, GLUK1) ensured that the effect described here was mediated solely by the kainate receptors. All experiments described here were done in the presence of TTX and GYKI, thus blocking both all action potentials in the slice (via the TTX) and all excitatory AMPA receptors (via the GYKI). Blocking all action potentials with the TTX effectively reduces neurotransmitter release. Therefore, by using the kainate-selective compounds in conjunction with the AMPA-specific blocking agent, and in further conjunction with the TTX, we ensured that our results were kainate dependent [26]. Adding GABAzine (10 μM) to the cell did not affect either the oscillatory period or the ability to photomodulate the cell [see Fig. 3(d)], thereby negating the possibility of an ionotropic inhibitory feedback response regulating the oscillations. Similar tests were done to block glycine receptors, metabotropic excitatory and inhibitory receptors, and NMDA receptors (see Methods). In all cases, the addition of these blockers had no effect on the ability of the cell to oscillate, or the ability to photomodulate the cell (at least $n = 2$ cells per drug study). These tests were done to verify that the effect described was an inherent

response of the PN *in vitro*, and not the effect of other synchronization events in the neuronal network, as has been shown for the cerebellum [27] and cortical networks [28].

C. Delayed recovery of modulation

The dynamics of the recordings subsequent to the photomodulation were also studied. Figure 4(a) displays a representative recording from a PN that was initially oscillating at a natural period of 22 s [green (light gray) curve], and then photomodulated for 2 min at 5 s on/ 5 s off [10 s period, blue (dark gray) curve], and subsequently allowed to recover (black curve). The PN faithfully follows the forced modulation after 1–2 stimuli when the light is applied, and then slowly recovers back to the natural oscillation period it had prior to the stimulation, after the photostimulation is stopped. This recovery response of the cell's oscillatory modulation is similar to a traditional forced oscillator, with an exponential recovery after the forced modulation is stopped. This is best visualized when plotting out the period and DC over time, as in Figs. 4(b) and 4(c), which display both the period matching during forced oscillation (dashed blue line) as well as the exponential recovery (dotted red line).

The time constants for recovery have a distribution among different cells, with a recovery time of 82 $\pm$ 48 s for the period, and 70 $\pm$ 41 s for the DC. ($n = 11$ cells. Errors are in SD, displaying the range of variation among cells.) The long recovery time for this process is similar to other forms of short-term memory in the brain (such as short-term
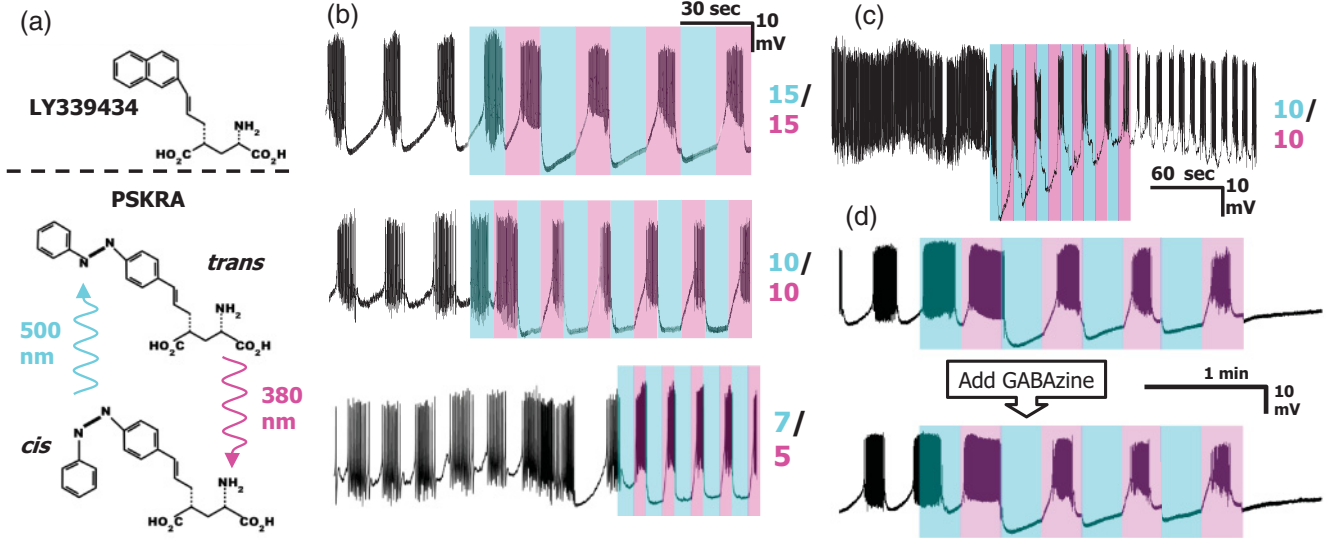
FIG. 3. (Color online) Photoswitchable compound modulates the oscillation. (a) Comparison of the GluK1 selective compound LY339434 and the PSKRA, which has an added azobenzene moiety, rendering it photoswitchable at 500 and 380 nm. (b) The ultraviolet [UV, 380 nm, as shown in violet (light gray) area] and cyan [500 nm, as shown in cyan (dark gray) area] light turn the bursting on and off, respectively, as a function of the modulation period, here shown for two modulation patterns with differing periods. The stimulation pattern is noted to the right of each recording, with stimulations at 15 s cyan, 15 s UV; 10 s cyan, 10 s UV (DC = 50%); and 7 s cyan, 5 s UV (DC = 42%). (c) Photomodulation followed by induction of oscillation in a cell not displaying astability prior to the modulation. The cell continued to oscillate after the photoswitching was completed. (d) Adding synaptic blockers to the solution (such as GABAzine, 10 μm, which blocks GABA receptors) did not affect any of the photoswitching, resulting in identical traces before and after introducing the drugs, verifying the kainate mediated effect.

depression [1,5]), allowing the cell to "remember" its forced modulation for a short duration after the stimulus is applied, however, the cells typically did not retain the forced frequency. The direction of recovery was generally toward the natural astable period in the cell prior to photomodulation, with forced photomodulation of the cells done both below and above their natural period [below: 5/5 s on/off modulation, $n = 7$; above: 10/10 s on/off modulation, $n = 9$; 15/15 s on/off modulation, $n = 4$, with representative cell recordings in Figs. 4(d) and 4(e), respectively].

IV. PARAMETRIC OSCILLATOR MODEL

The bursting oscillations of the PNs are nondissipating, with a clear frequency signature in the FFTs. We can simplify the Hodgkin-Huxley equations [29–32] to reach a model similar to the fundamental parametric oscillator equations to describe this slow harmonic signal. This derivation can be applied to any cell exhibiting slow rhythmic bursting, such as sleep spindles [33], and is particularly applicable to the known slow oscillatory firing patterns of the PN [16,30,34]. The generalized formula for the membrane potential V, injected current I, and membrane capacitance C, is [30,31]

$$C\dot{V} = -I - \sum g_i x_i^{ki}(V - E_i), \qquad (1)$$

with each gating variable x_i, being a function of the voltage: $\dot{x}_i = [x_{0i}(V) - x_i]/\tau_i(V)$, which is a generalized differential form for the gating variable as a function of the asymptotic value of the gating variable x_{0i}, and a generalized time constant τ_i [32]. In Eq. (1), g_i is the conductance per ion channel and

the $(V - E_i)$ term is the driving force per ion channel. Taking a time derivative of Eq. (1) results in

$$C\ddot{V} = -\dot{I} - \sum \left[\dot{g}_i x_i^{ki}(V - E_i) + g_i \frac{d(x_i^{ki})}{dt}(V - E_i) \right. $$
$$\left. + g_i x_i^{ki}\dot{V} \right]. \qquad (2)$$

Assuming that the injected current (I, if any exists) is constant with time, and that the conductance coefficients g_i are also time independent, we can neglect the dI/dt and dg_i/dt terms, remaining with

$$C\ddot{V} = -\sum \left[g_i \frac{d(x_i^{ki})}{dt}(V - E_i) + g_i x_i^{ki}\dot{V} \right]. \qquad (3)$$

Since we are interested in the slow changing terms only, whose changes with time are of the order of the oscillation period (10–25 s), we can isolate these terms by removing them from the summation:

$$C\ddot{V} = -g_S \frac{d(x_S^s)}{dt}(V - E_S) - g_S x_S^s \dot{V}$$
$$- \sum_{\text{fast}} \left[g_i \frac{d(x_i^{ki})}{dt}(V - E_i) + g_i x_i^{ki}\dot{V} \right]. \qquad (4)$$

In Eq. (4), the slow gating variable g_S has an exponent of s. We will assume that this exponent is unity, since the slow action of our experimental results is somewhat similar
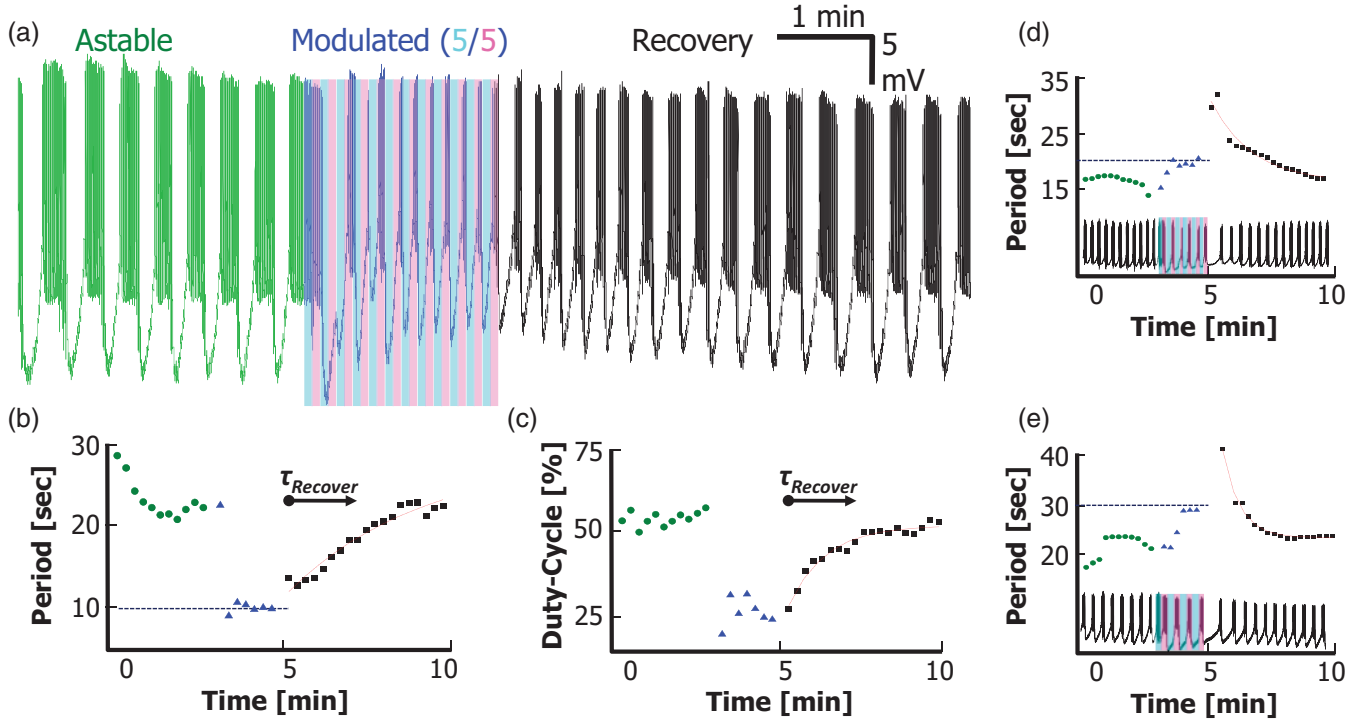
FIG. 4. (Color online) Recovery from the photomodulation follows a forced-oscillator model. (a) Exemplary recording of a Purkinje neuron showing a natural oscillation [green (light gray) curve] that is then photomodulated at 5 s on [violet (light gray) area] /5 s off [cyan (dark gray) area] with a 10 s period for 2 min [blue (dark gray) curve], and then allowed to recover from the modulation (black curve). [(b), (c)] Period and duty-cycle tracking of the cell in (a), displaying the forced-modulation (dashed blue line) and exponential recovery. Dots are color coded as in (a). Red dotted lines are fitted exponential curves for the recovery segment, with a time constant of $\tau = 124$ s and $\tau = 67$ s for the period and duty cycle, respectively. [(d), (e)] Representative plotted periods of the natural, modulated, and recovering oscillators for two different modulations: (d) 10/10 and (e) 15/15 on/off, in seconds ($\tau = 97, 40$ s, respectively). Actual recordings appear below each plot.

to that of either the muscarinic gating variable M, or h for the I_h refractory current, both of which have an exponent of unity [30,31].

The rightmost bracketed term in the summation can be taken as the *average value* for long periods where the fast acting terms within these brackets change at a rate that is much higher than the slow oscillations examined here. This is because the time derivative d/dt for long time durations is defined by changes of the order of $1/T = f_S$, which is the switching frequency of the cell. This is comparable with taking the average membrane potential during the firing of action potentials, otherwise known as the "up" state of a bistable system [16], such that we are dealing only with a *slow* wave form that is similar to a square-wave envelope [as shown in the inset of Fig. 1(a)]. With these assumptions, we obtain

$$C\ddot{V} = -g_S\dot{x}_S V + g_S\dot{x}_S E_S - g_S x_S \dot{V}$$
$$- \left\langle \sum_{\text{fast}} \left[g_i \frac{d(x_i^{ki})}{dt}(V - E_i) + g_i x_i \dot{V} \right] \right\rangle_{\text{avg}}. \quad (5)$$

The middle term $g_S\dot{x}_S E_S$ can further be isolated, since it is a term that is directly dependent upon the time, but only indirectly on the voltage. Reorganizing the above equation, we can obtain a generalized second-order differential

equation:

$$C\ddot{V} + g_S x_S \dot{V} + g_S\dot{x}_S V$$
$$= g_S\dot{x}_S E_S - \left\langle \sum_{\text{fast}} \left[g_i \frac{d(x_i^{ki})}{dt}(V - E_i) + g_i x_i \dot{V} \right] \right\rangle_{\text{avg}}. \quad (6)$$

Or, if we replace the time average of the faster spikes with a constant

$$C\ddot{V} + g_S x_S \dot{V} + g_S\dot{x}_S V \approx g_S\dot{x}_S E_S + \langle \text{const} \rangle_{\text{avg}}. \quad (7)$$

Comparing this to the harmonic oscillator with a driven source, $F(t)$ [35]:

$$m\ddot{V} + b\dot{V} + kV = F(t). \quad (8)$$

Equation (8) is the classic equation for a *driven harmonic oscillator* with a resonant frequency of $\omega_0^2 = k/m$ and a quality factor of $Q = \omega_0 m/b$, with $F(t)$ being the time-dependent driving input. Comparing terms, we find that

$$m = C, \quad b(V,t) = g_S x_S, \quad k(V,t) = g_S\dot{x}_S. \quad (9)$$

As can be seen, the parameters of this equation are *time/voltage dependent*. This makes the equation a *parametric oscillator* as opposed to a simple *harmonic* oscillator. The

parameters in Eq. (9) are related to the biological and measurable aspects of each neuron, with the membrane capacitance directly measurable, and the gating variables measurable using voltage-clamp experiments to determine the dynamics of the ion channels involved.

If the oscillator is underdamped ($Q > 1/2$, which is equivalent to $b \ll \omega_0$), it is easy to then measure the resonance frequency of the Purkinje neuron ($2\pi f_0 = \omega_0$) as well as the quality factor Q, from the signal-to-noise ratio (SNR). The frequency of an oscillating Purkinje neuron can be measured directly in the frequency domain, and the SNR can be calculated either through the time-tracking algorithm, or from the width of the peak in the FFT. The frequency of the damped oscillator, which is the experimentally measured switching frequency $\omega_S = 2\pi f_S$, is related to the resonance frequency

$$\omega_0^2 = \omega_S^2/[1 - 1/(4Q^2)], \qquad (10)$$

with Q taken as the SNR. For highly precise oscillating neurons with $Q > 2$: $\omega_S \approx \omega_0$. Therefore, by measuring these two parameters (f_S and Q), and taking a general value of the membrane capacitance of $C = 1\ \mu\text{F/cm}^2$ [31], we can obtain estimations for the parameters k and b. This value of the membrane capacitance is used to provide an order-of-magnitude estimation of the relevant parameters.

Equation (7) is the parametric oscillator equation for an oscillating neuron that can be analyzed using phase-space diagrams [32]. Obtaining the van der Pol oscillator equation from the Hodgkin-Huxley equations follows a similar method. Floquet analysis posits that the signal of the oscillation should vary similarly to the source. Since the measured signal from the cell is periodic in time, we can inversely infer that the gating variable is also periodic, with the same frequency. Equation (7) therefore gives the driving force of the parametric oscillation as a function of the gating variable.

V. DATA ANALYSIS

The period (1/frequency) and DC of the astable mode were measured in $n = 43$ cells, each oscillating for at least 3 min, and are displayed in Figs. 5(a) and 5(b). Since each cell acts as an independent oscillator, it is expected to find a range of inherent frequencies. We found that the average period of the cells was 20 ± 8 s, and the average DC was $46 \pm 8\%$ ($\pm$ SD). We again note the similarity between the range of slow oscillations measured here, and those measured *in vivo* in PNs in tottering mice, which ranged between 12.82 and 25.64 s [15]. There appears to be a slight increase in the period with the application of the SYM-2081/MSG in comparison to the PSKRA (24 ± 7 vs 19 ± 8 s; verified with a two-tailed t test, assuming unequal variance, $p < 0.013$). The cause of this variation may be due to the concentrations used, as low concentrations of SYM-2081 ($10\ \mu$M) did not induce oscillations, but only continuous Ca^{2+} spikes, and that the effective "active" concentration of $100\ \mu$M PSKRA in the dark is not uniquely defined [20].

The precision of oscillation over time can be measured by the quality factor of the resonator Q or the SNR. This was measured using the window-tracking algorithm in the time domain, for each of the cells measured, and displayed in Fig. 5(c) for each individual cell. Of the PSKRA activated cells, 45% [$n = 13/29$, blue (dark gray) circles] had a SNR larger than 10, corresponding to less than a 10% deviation in period over time, whereas the SYM-2081/MSG activated cells were less accurate [green (light gray) triangles]. This may be attributable to either the selectiveness of the PSKRA, or the concentration ratios.

Using the formalism of the parametric oscillator above, we can view each PN as an independent oscillator, each with its own measurable parameters of oscillation. To obtain an order of magnitude approximation for the channel conductance, we can use the time and voltage averaged value for the gating variable, which is normalized to vary between 0 and 1 [32], such that $\langle x_S \rangle \approx 0.5$. Therefore, using Eq. (9), we can relate the measured quantities to find the conductance: $\langle b \rangle = g_S \langle x_S \rangle \approx$
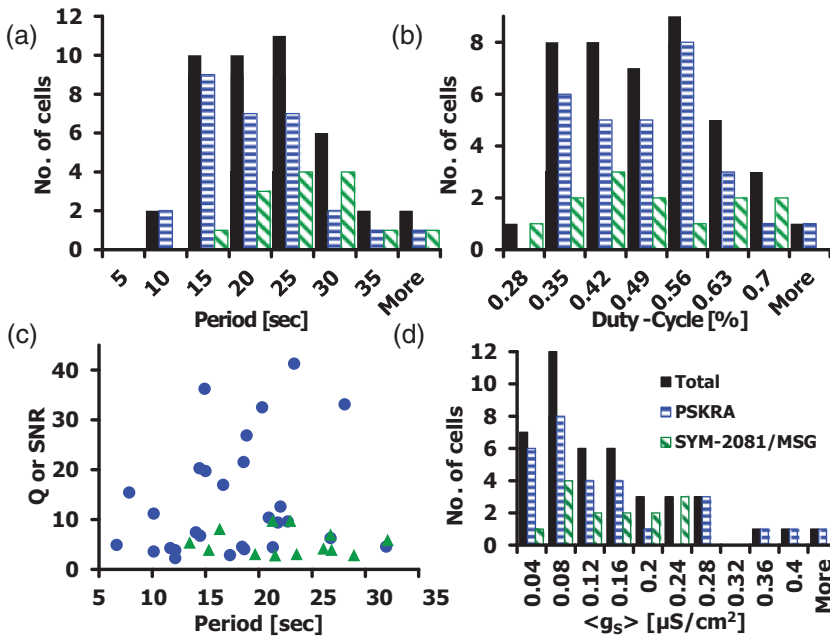

FIG. 5. (Color online) Period, duty-cycle, and precision of oscillation. [(a), (b)] Histograms of the average period and duty cycle ($n = 43$ cells total) showing the central frequency of 20 s/0.05 Hz, and 46% duty cycle in total (black). The cells could be broken down to PSKRA activated cells (horizontal blue, $n = 29$) and SYM-2081/MSG activated cells (diagonal green, $n = 14$), with periods of 24 ± 7 and 19 ± 8, respectively. (c) Quality factor or SNR data for the PSKRA [blue (dark gray) circles] and SYM-2081/MSG [green (light gray) triangles] activated cells, as a measure of the precision of oscillation. Each cell is plotted individually, with the PSKRA activated cells having higher precision values. (d) Histogram of the time averaged value of the slow gating variable for each cell. The average value of $\langle g_S \rangle$ was 0.12 ± 0.1 $\mu\text{S/cm}^2$.

$g_S/2$ and $b = C\omega_0/Q$ from the experimental measurements. This procedure provides an order-of-magnitude result only, since each cell has its own membrane capacitance, and since a substantial number of approximations were used to obtain the relationship in Eq. (9).

Implementing this calculation on the $n = 43$ cells for the time-averaged gating variable for each cell is displayed in Fig. 5(d). Each oscillator is independent, with an average channel conductance of $\langle g_S \rangle = 0.12 \pm 0.1 \ \mu\text{S/cm}^2$. Once again the SD is of the same order as the mean, signifying that this average value provides a wide range for the conductance. This value of channel conductance is far smaller than those of existing channels listed for the PN, which are as low as 30–300 $\mu\text{S/cm}^2$ for g_h [30,36] and 40–750 $\mu\text{S/cm}^2$ for g_M [31,36], both of which are known to activate on scales of roughly under 1 s. The relationship between the h current and bistability has previously been shown for PNs with similar time scales of switching [16], as well as in 1–2 Hz rhythmic bursts in thalamic relay neurons, which have $g_h = 0.015$–$0.03 \ \mu\text{S}$ (not normalized to cm^2) [37]. Due to the units of the membrane capacitance ($\mu\text{F/cm}^2$) and low frequency of astability, the values for the conduction are quite low, and match the low frequency of oscillation of these PNs. Since the time scale of these astable oscillations is orders of magnitude longer than those of Na$^+$ and Ca^{2+} spikes, and since the kainate receptors which mediate this effect only comprise ∼5% of the ionotropic glutamate receptors on the PN [38], this low conductivity channel would appear to describe a conduction pathway that is not currently incorporated into existing PN models [30,31,36,39].

VI. CONCLUSIONS

This work has shown the capability of a PN to act as an astable oscillator with long periods of oscillation (10-25 s), as well as the ability to externally tune this frequency for extended periods of time. This frequency range is notably outside the range typically studied in the brain [11–14], but matches other *in vivo* results of the PN [15]. The approximate range of the channel conductance mediating this oscillation was also shown to be outside that of the traditionally modeled channels [39].

This work describes a new functional role for the PN, that of an astable oscillator in the cerebellum. The astable oscillator is the basic form of clock for most modern circuits [10], and the long periods of the bursting mode described in Figs. 1 and 2 correspond to a timing cycle that is outside the realm of frequencies typically studied in other parts of the brain [11,12], as well as in the cerebellum itself [14]. The long periods measured here lie in the region of temporal recognition that is between the realm of high-frequency action potentials and our own conscious thought [40], and similar timing modes in other regions of the brain should be searched for in order to parallel this newfound capability of the PN in the cerebellum. The KRA induction of this clocking mode is quite different from the well-known induction of gamma frequencies (30–80 Hz) in other parts of the brain [41]. The similarity with those faster oscillations is comparable to our analysis of the calcium frequency (1–15 Hz) in the PN [9], which is closer to the theta frequency band (5–10 Hz) [11]. While we had previously shown calcium frequency activation using the

KRA ATPA, as well as a partial modulation capability of the calcium frequency with the PSKRA [9], we here show that the kainate receptor activation using PSKRA and SYM-2081 (both molecular variants of each other [20,22]) can reliably induce and modulate the switching frequency, which is here denoted as the astability frequency. Furthermore, while we had previously shown inherent switching frequencies only in some *in vitro* "control" preparations, this work demonstrates that nearly every PN can be induced into an astable state under the influence of certain KRAs. There have been no other reports of sub-1 Hz kainate induced oscillations in any region of the brain.

The ability to tune this clock externally adds another dimension to this paradigm, since it allows a variable clock speed to be considered. This would be an essential characteristic of a dynamic control system, which the cerebellum is theorized to act as [1,6,24]. This short duration entraining of the switching frequency can be accomplished externally using synaptic transmission, which was here emulated with the PSKRA. It is unknown if there is a similar long-term memory capability for plastically changing the rhythm of this astable behavior.

The assumed existence of such a timing functionality of the PN in the cerebellum also lies in complete agreement with temporal pattern generator theories of the cerebellum [24]. We have previously postulated that the PN can act as the basic timing circuit for the cerebellum [10], since it has demonstrated both monostability and bistability, and is here shown to exhibit both constant and tunable astability. Since a temporal pattern generator would require the ability to combine a full range of frequencies, the three frequency ranges of the PNs [9] can help recreate nearly any mathematical signal via inverse Fourier expansion.

The source of the slow oscillation was here described in terms of the possible periodic gating variable dynamics of the parametric oscillator model, as well as the dependence upon the poorly understood kainate receptors in the PN [26]. This can be compared with a parametric variation of the resistors and capacitors connected to a multivibrator circuit, which can transition such a circuit between astable, bistable, and monostable modalities (see Fig. 5 in Ref. [10]). The transition between each of these modalities would be possible via an external modification to the PN's inputs, such as is known to occur with the climbing fiber input to the PN, which can toggle the bistability of the PN's membrane voltage [16–18]. We here showed the induction of the astable modality using KRAs, which are typically not considered in most PN models. The activation of astable oscillations in cells such as in Fig. 3(c) signifies that the inherent capability of the PN to oscillate may need to be externally activated, perhaps via the surplus of glutamate in the synaptic clefts, which would activate all the kainate receptors on the cell. Both the parametric oscillator and multivibrator circuit models predict this phenomenon, since a parametric oscillator will only begin to oscillate once its parameters are initially perturbed, and an astable multivibrator circuit will only oscillate once one of its external components are thermally perturbed. Using mathematical dynamic systems, circuit modeling and newly derived optical activation techniques [25] will allow us to probe the intrinsic behavior of cells within a network, thereby

enabling us to reverse engineer the neuronal circuitry of the brain at a higher complexity.

[1] M. Ito, Prog. Neurobiol. **78**, 272 (2006).

[2] J. C. Eccles, M. Ito, and J. Szentágothai, *The Cerebellum as a Neuronal Machine* (Springer-Verlag, Berlin, 1967).

[3] D. Marr, J. Physiol. London **202**, 437 (1967).

[4] J. S. Albus, Math. Biosci. **10**, 25 (1971).

[5] M. Ito, Physiol. Rev. **81**, 1143 (2001).

[6] K. Doya, H. Kimura, and M. Kawato, IEEE Control Syst. Mag. **21**, 42 (2001).

[7] D. Rokni, R. Llinás, and Y. Yarom, Front Neurosci. **2**, 192 (2008).

[8] J. M. Bower, Front. Cell. Neurosci. **4**, 27 (2010).

[9] Z. R. Abrams, A. Warrier, D. Trauner, and X. Zhang, Front. Neur. Circ. **4**, 13 (2010).

[10] Z. R. Abrams and X. Zhang, Front. Neur. Circ. **5**, 11 (2011).

[11] G. Buzsáki and A. Draguhn, Science **304**, 1926 (2004).

[12] M. Steriade, Neuroscience **137**, 1087 (2006).

[13] A. K. Roopun, M. A. Kramer, L. M. Carracedo, M. Kaiser, C. H. Davies, R. D. Traub, N. J. Kopell, and M. A. Whittington, Front. Neurosci. **2**, 145 (2008).

[14] C. I. De Zeeuw, F. E. Hoebeek, and M. Schonewille, Neuron **58**, 655 (2008).

[15] G. Chen, L. S. Popa, X. Wang, W. Gao, J. Barnes, C. M. Hendrix, E. J. Hess, and T. J. Ebner, J. Neurophysiol. **101**, 234 (2009).

[16] Y. Loewenstein, S. Mahon, P. Chadderton, K. Kitamura, H. Sompolinsky, Y. Yarom, and M. Haüsser, Nat. Neurosci. **8**, 202 (2005).

[17] B. E. McKay, J. D. T. Engbers, W. H. Mehaffey, G. R. J. Gordon, M. L. Molineux, J. S. Bains, and R. W. Turner, J. Neurophysiol. **97**, 2590 (2007).

[18] M. Yartsev, R. Givon-Mayo, M. Maller, and O. Donchin, Front. Syst. Neurosci. **3**, 1 (2009).

[19] M. Schonewille, S. Khosrovani, B. H. J. Winkelman, F. E. Hoebeek, M. T. G. De Jeu, I. M. Larsen, J. Van Der Burg, M. T. Schmolesky, M. A. Frens, and C. I. De Zeeuw, Nat. Neurosci. **9**, 459 (2006).

[20] M. Volgraf, P. Gorostiza, S. Szobota, M. R. Helix, E. Y. Isacoff, and D. Trauner, J. Am. Chem. Soc. **129**, 260 (2007).

[21] A. L. Hodgkin and A. F. Huxley, J. Physiol. **117**, 500 (1952).

[22] B. Small, J. Thomas, M. Kemp, K. Hoo, B. Ballyk, M. Deverill, A. M. Ogden, A. Rubio, C. Pedregal, and D. Bleakman, Neuropharmacology **37**, 1261 (1998).

[23] J. Hartmann and A. Konnerth, Cell Calcium **37**, 459 (2005).

[24] G. A. Jacobson, D. Rokni, and Y. Yarom, Trends Neurosci. **31**, 617 (2008).

[25] T. Fehrentz, M. Schönberger, and D. Trauner, Angew. Chem., Int. Ed. **50**, 2 (2011).

[26] D. E. Jane, D. Lodge, and G. L. Collingridge, Neuropharmacology **56**, 90 (2009).

[27] G. A. Jacobson, D. Rokni, and Y. Yarom, Trends Neurosci. **31**, 617 (2008).

[28] I. Baruchi, V. Volman, N. Raichman, M. Shein, and E. Ben-Jacob, Eur. J. Neurosci. **28**, 1825 (2008).

[29] C. Morris and H. Lecar, Biophys. J. **35**, 193 (1981).

[30] F. R. Fernandez, J. D. T. Engbers, and R. W. Turner, J. Neurophysiol. **98**, 278 (2007).

[31] M. A. Kramer, R. D. Traub, and N. J. Kopell, Phys. Rev. Lett. **101**, 068103 (2008).

[32] E. M. Izhikevich, *Dynamical Systems in Neuroscience: The Geometry of Excitability and Bursting* (MIT Press, Cambridge, MA, 2006).

[33] M. V. Sanchez-Vives and D. A. McCormick, Nat. Neurosci. **3**, 1027 (2000).

[34] W. Chang, J. C. Strahlendorf, and H. K. Strahlendorf, Brain Res. **614**, 335 (1993).

[35] L. S. Borkowski, Phys. Rev. E **83**, 051901 (2011).

[36] E. De Schutter and J. M. Bower, J. Neurosci. **71**, 375 (1994).

[37] J. R. Huguenard and D. A. McCormick, J. Neurophys. **68**, 1373 (1992).

[38] Y. H. Huang, M. Dykes-Hoberg, K. Tanaka, J. D. Rothstein, and D. E. Bergles, J. Neurosci. **24**, 103 (2004).

[39] P. Achard and E. De Schutter, Front. Comput. Neurosci. **2**, 8 (2008).

[40] D. V. Buonomano, Nat. Chem. Biol. **3**, 594 (2008).

[41] A. Fisahn, J. Physiol. **562**, 65 (2005).